Chimica Techno Acta
published by Ural Federal University
eISSN 2411-1414
chimicatechnoacta.ru

ARTICLE
2023, vol. 10(4), No. 202310407
DOI: 10.15826/chimtech.2023.10.4.07

Facile synthesis of lanthanum-doped $SrTiO_3$ nanocubes mediated by cetyltrimethylammonium bromide and tert-butylamine under solvothermal condition and their tunable electrical properties

Yulia Eka Putri [a]*, Humaira Faradilla [a], Dedi Satria [b], Diana Vanda Wellia [a]

a: Department of Chemistry, Faculty of Mathematics and Natural Science, Andalas University, Padang 25163, Indonesia
b: Department of Pharmacy, Faculty of Pharmacy, Muhammadiyah University of Sumatera Barat, Padang 25172, Indonesia
* Corresponding author: yuliaekaputri@sci.unand.ac.id

This paper belongs to a Regular Issue.

Abstract

The electrical conductivity of low concentrations of lanthanum-doped $SrTiO_3$ nanocube ceramics synthesized using the facile solvothermal method in mixed organic and inorganic solvents with cetyltrimethylammonium bromide (CTAB) as a capping agent and tert-butyl amine (TBA) as a mineralizer was investigated. X-ray diffraction patterns confirmed the formation of a high-purity perovskite phase, corresponding to the standard data and the pattern refinement results. The particles of the sample were nanocubes, whereas the La-doped $SrTiO_3$ sample particles were more uniform in size and shape, as shown in TEM images. The FT-IR spectrum confirmed the vibration of the CH_3-N^+ groups from CTAB and TBA, indicating an electrostatic interaction between their functional groups and the particle surface. Substitution of La^{3+} ions at low concentrations increased electrical conductivity compared to the undoped $SrTiO_3$ sample. Lanthanum donates excess electrons, thereby increasing the number of electron carriers, which causes a reduction in the band gap energy according to the UV-DRS spectrum analysis using the Tauc equation.

Keywords

strontium titanate
perovskite
doping
lanthanum
electrical conductivity

Received: 25.09.23
Revised: 16.10.23
Accepted: 17.10.23
Available online: 26.10.23

Key findings

- Synergistic effect of CTAB and TBA results in high crystallinity of La-doped $SrTiO_3$ nanocubes with uniform morphology.
- The narrowing of the band gap energy is associated with higher valence dopant substitution.
- Higher valence substitution is useful for increasing the electrical conductivity of the La-doped $SrTiO_3$ nanocubes.

1. Introduction

Nanomaterials have become means to overcoming the problem of realizing tunable electronic properties in bulk materials [1]. Controlling nanomaterials' shape, size, crystallinity, and surface is the main focus of creating their unique electronic, optical, mechanical, magnetic, and chemical properties regarding quantum confinement effects and large surface-to-volume ratios [2, 3]. Dresselhaus et al. reported a practical approach to improving material properties, i.e., forming nanoscale components that cause quantum confinement and scattering effects due to multiple internal interfaces [4]. This approach has proven effective in improving material properties in various advanced material applications. Utilizing nanoparticles with lower dimensions (2D/quantum wells, 1D/quantum wires, as well as 0D/quantum dots) with specific physical characteristics increases the electrical properties in 3D crystalline solids. The electrical properties of these materials depend on the number and arrangement of interacting atoms, ions, and molecules inside their crystal structure.

Nanoscience is a collection of methods, techniques, skills, and procedures for producing nano-size materials with their unique characteristics. One of the indispensable

nanomaterials is the oxide semiconductor. Nanostructured metal oxide semiconductors have found many practical applications [5]. Nanomaterials' physical, chemical, mechanical, optical, and electronic properties are applicable in various fields such as sensor [6], catalytic [7], optical ceramics [8], food processing [9], and energy conversion materials, namely dye-sensitized solar cells [10] and thermoelectric materials [11].

Among the vast multitude of oxide semiconductors that have been reported on strontium titanate ($SrTiO_3$) nanomaterial is one of the classic oxide types that have attracted technological interest as electronic materials. The extensive utilization of $SrTiO_3$ as electronic material is mainly due to its flexible crystal structure and a wide range of tunable morphological geometries [12]. Strontium titanate has an ideal perovskite structure (ABO_3) represented by a cubic unit cell [13]. Its ideal cubic unit cell structure can be modified by introducing foreign ions in the crystal, affecting the electronic band structure and producing a new electronic behaviour [14]. On the other hand, the cubic shape of the $SrTiO_3$ provides a larger interface for the self-assembly of nanoparticles, resulting in a well-defined morphology.

$SrTiO_3$ is a semiconductor with a broad band gap, namely an indirect band gap of 3.25 eV and a direct band gap of 3.75 eV, which can be tailored by substitution at the Sr- or Ti-site to increase the number of carriers. Substitutional doping can control the carrier concentration of $SrTiO_3$ to improve the electronic properties [15]. Improving the carrier concentration through a higher valence dopant for A- and B-sites in the perovskite structure can be accomplished by substituting transition elements in the $SrTiO_3$ lattice. The substitution of lanthanum ions (La^{3+}) and niobium ions (Nb^{5+}) in $SrTiO_3$ was reported as a potential strategy to introduce electron donors, leading to an increase in the concentration of electron carriers and, consequently, an increase in electrical conductivity [16, 17]. Furthermore, the electrical conductivity is affected by carrier concentration and mobility due to changes in the electronic structure [18].

It is widely reported that metal oxides produced by the solvothermal process exhibit a high crystallinity and smaller particle sizes with narrower particle distribution. The synthesis parameters, such as molar ratios, solvents, additives, and synthesis temperature and time, significantly affect the purity and morphology of resulting particles [19]. In our previous work, we successfully synthesized highly polycrystalline samples of $SrTiO_3$ nanocubes via the solvothermal method, utilizing CTAB and TBA's synergistic effect as a capping agent and mineralizer [20]. $SrTiO_3$ nanocubes demonstrated distinguishing characteristics related to their shape, namely the phenomenon of surface scattering to introduce new functionalities. The formation of nanocubes can significantly reduce the heat conduction of $SrTiO_3$ through the phonon scattering mechanism so that the electrical conductivity does not change. In addition, the electrical conductivity of $SrTiO_3$ can still be improved while maintaining its cubic shape so that $SrTiO_3$ nanocubes retain their superior properties of high electrical conductivity but low thermal conductivity. This unique property of $SrTiO_3$ allows its potential application as a thermoelectric material [21].

In this work, the substitution of lanthanum ions (La^{3+}) as electron donors to strontium-sites in perovskite $SrTiO_3$ nanocubes was carried out using the solvothermal method in mixed inorganic-organic solvents of water and ethanol-isopropanol. A series of La-doped $SrTiO_3$ samples were prepared. Their crystal structure, morphology, and molecular interaction were characterized using X-ray diffraction, transmission electron microscopy (TEM), and Fourier transform infrared spectroscopy (FT-IR). The effect of lanthanum substitution on the electrical conductivity was also investigated by measuring the electrical resistivity using an LCR meter and the optical response using UV-vis Diffuse Reflectance Spectroscopy (UV-DRS).

2. Experimental procedures

2.1. Materials

Titanium tetraisopropoxide (TTIP), lanthanum nitrate hexahydrate ($La(NO_3)_3{\cdot}6H_2O$), cetyltrimethylammonium bromide (CTAB), tert-butylamine (TBA) were bought from Sigma-Aldrich Chemical Reagent Co., with high purity ≥99.9%. Strontium nitrate ($Sr(NO_3)_2$), sodium hydroxide (NaOH), ethanol p.a, and isopropanol p.a were bought from Merck & Co., Inc. (purity ≥ 99%). All of the chemicals were applied without any further purification.

2.2. Synthesis of La-doped $SrTiO_3$ nanocubes

Synthesis was conducted by preparing a TTIP solution in a mixture of solvents (ethanol: isopropanol) while stirring for 10 min at a speed of 300 rpm. After the dissolution, 1.0 M NaOH was added, and the mixture was stirred for 10 min until the formation of a suspension with a pH of 14. Then $Sr(NO_3)_2$ was added to the suspension, which was placed in an ice bath while stirring for 20 min to form a homogeneous white solution. CTAB was added to the solution with a mole ratio of STO:CTAB of 1:0.5 upon stirring for 1 h. Then, 1 mole of TBA was added followed by stirringfor 10 min. After that, the white solution was put into a teflon vessel and placed in a Parr bomb model. The solvothermal process was carried out in an oven at 220 °C for 72 h. Next, the suspension was cooled at room temperature and washed using distilled water and ethanol through decantation. The precipitate was dried in an oven at 105 °C for 5 h, forming $SrTiO_3$ powder, and the sample was labeled STO. Likewise, samples prepared by adding lanthanum in different amounts to form $Sr_{1-x}La_xTiO_3$ (x = 0.025, 0.05, 0.075, 0.1) were also prepared using the same synthesis procedure. $La(NO_3)_3$ was added to the solution after $Sr(NO_3)_2$. The La-doped $SrTiO_3$ samples were labeled as SLTO-0.025, SLTO-0.05, SLTO-0.075, and SLTO-0.1, respectively.

 DOI: 10.15826/chimtech.2023.10.4.07

2.3. Characterization

The phases and crystal structures were characterized using X-Ray Diffraction (XRD; PANalytical X-pert PRO) with Cu Kα radiation at room temperature. XRD measurements of the synthesized powder were carried out in the range of 20–65° with a scanning rate of 0.5°/second. The XRD data was subsequently refined using the Le Bail technique to determine the crystal system and unit cell parameters using the Rietica software. The interaction of functional groups in the samples can be determined by Fourier transform infrared spectroscopy (PerkinElmer type FT-IR Spectrometer Frontier). The morphology of the samples was observed using a High Magnification Transmission Electron Microscope (HM-TEM; Tecnai G2 20S-Twin Function). The bandgap energy was calculated by the sample's absorption in the UV and visible light regions using ultraviolet-visible diffuse reflectance spectroscopy (UV-vis DRS; Analytic Jena SPECORD 210 PLUS). Meanwhile, the electrical conductivity value was calculated using the resistivity value measured from the LCR meter (Motech MT 4099).

3. Results and Discussions

The crystallinity and crystal structure identification for all synthesized samples was carried out by analyzing the XRD patterns of the samples and comparing them with the standard data (ICSD-94573), as shown in Figure 1. The XRD patterns of $SrTiO_3$ and La-doped $SrTiO_3$ samples were similar to the standard data. However, the crystallinity of the samples decreased as the lanthanum concentration increased, as indicated by the decrease and broadening of the main diffraction peak (110) height and width, respectively. The enlarged XRD patterns at the (110) peak slightly shifted towards the higher 2θ for all polycrystalline samples when the La^{3+} ion was substituted into the Sr^{2+} site, corresponding to the decrease in the lattice parameters and unit cell volume. The lattice distortion within the crystal structure caused the changes in the crystal structure as lanthanum ions have smaller ionic radii (1.36 Å) compared to the strontium ions (1.44 Å) [22]. As a result, the higher concentration of lanthanum dopant induced lower crystallinity and resulted in the formation of a $SrCO_3$ impurity.

The crystallinity of the $SrTiO_3$ samples is related to the dissolution of the TTIP molecules in the mixed solvent of ethanol and isopropanol for stabilizing $[Ti(OH)_6]^{2-}$ ions. In turn, the stabilized $[Ti(OH)_6]^{2-}$ ions facilitate the diffusion of Sr^{2+} cations and initiate nucleation, thus leading to the $SrTiO_3$ crystal growth stage [23]. Utilizing mixed inorganic and organic solvents (water-ethanol-isopropanol) with low viscosity will enhance the ion diffusion rate in the reaction, making it easier to initiate the nucleation stage to form larger $SrTiO_3$ nuclei. Carbon dioxide in atmospheric air promotes the formation of $SrCO_3$ as a secondary phase during synthesis, which interferes with the formation of the perovskite phase. The solubility of lanthanum in strontium titanate is low, limiting higher La^{3+} ions concentrations in the host perovskite lattice. Moreover, lanthanum can form a secondary phase with oxygen at higher doping concentrations. Therefore, lanthanum causes significant alterations in the structural properties of $SrTiO_3$ perovskite [24].

Refinement analysis using the Le Bail method determines the structural properties of the final products. This analysis was carried out in this work to investigate the effect of lanthanum doping on the $SrTiO_3$ structure using the cubic phase parameters with the space group *Pm3m* as the initial model. The refinement profiles of the polycrystalline $SrTiO_3$ samples are shown in Figure 2, along with the difference curves between the Le Bail refinement pattern and the diffraction pattern of the prepared samples. The existence of low peaks, which were not fitted for all samples, was identified as an impurity phase of $SrCO_3$. The La^{3+} ions substitution for Sr^{2+} ions in the $SrTiO_3$ lattice resulted in the lattice parameters and volume cell variation for all samples as displayed in Table 1. The lanthanum substitution caused the shortening of the lattice parameters, thereby decreasing the unit cell volume, which signified the successful lanthanum substitution at the strontium sites. The La-doped $SrTiO_3$ diffraction peaks had a low discrepancy factor (R_p, R_{wp} < 5%), indicating that the Le Bail refinement analysis showed a good fit for all the samples. Moreover, all diffraction peaks were indexed with the Bragg reflection, indicating that low concentrations of lanthanum-doped $SrTiO_3$ samples were single-phase products that adopted the cubic *Pm3m* structure [17].

The refinement results prove that substituting low concentration of lanthanum in $SrTiO_3$ does not change the crystal structure of $SrTiO_3$. As a result, the STO and SLTO-0.025 samples were selected for further characterization, observation, and measurements.

The morphology of the STO and SLTO-0.025 samples, as shown in Figures 3a and 3b, portray a nano-sized, uniform cubic particle shape. The well-defined nanocube morphology can be controlled by adjusting the parameters of the solvothermal synthesis.

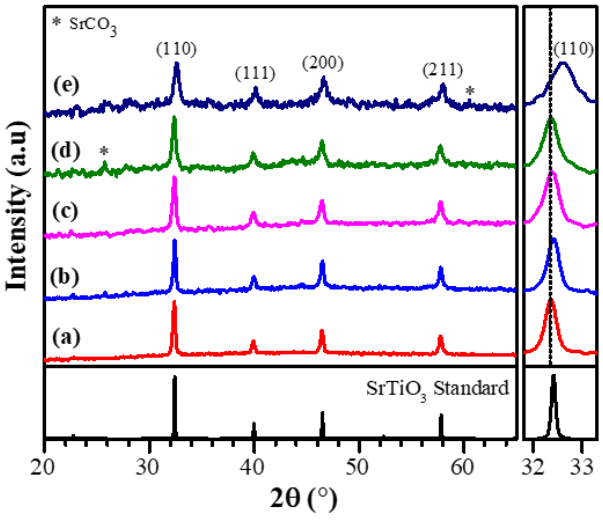

Figure 1 XRD patterns of La-doped $SrTiO_3$ samples, STO (a), SLTO-0.025 (b), SLTO-0.05 (c), SLTO-0.075 (d), SLTO-0.1 (e) and magnified (110) main diffraction peak.

 DOI: 10.15826/chimtech.2023.10.4.07

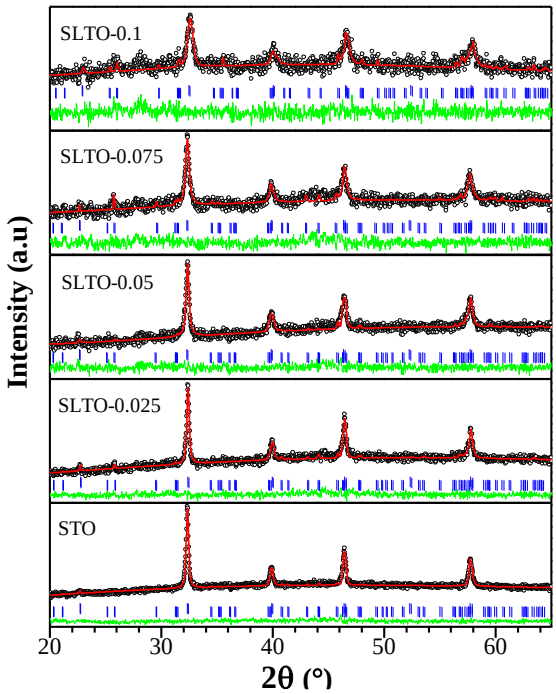

Figure 2 Le Bail refinement of the structural model for all $SrTiO_3$ samples; experimental XRD data (black open circles), calculated data (red line), and the difference patterns between obtained XRD data and the Le Bail refined (green line). The blue tick marks indicate the positions of allowed Bragg reflections in the space group *Pm3m*.

Table 1 Refined structural parameters of $SrTiO_3$ samples with different lanthanum content.

Parameter	STO	SLTO-0.025	SLTO-0.05	SLTO-0.075	SLTO-0.1
Space group	*Pm3m*	*Pm3m*	*Pm3m*	*Pm3m*	*Pm3m*
Crystal Class	Cubic	Cubic	Cubic	Cubic	Cubic
$a=b=c$ (Å)	3.9077	3.9063	3.9030	3.9063	3.9155
V (Å^3)	59.673	59.606	59.454	59.606	60.027
Z	1	1	1	1	1
R_p (%)	2.40	2.62	2.77	3.07	3.85
R_{wp} (%)	3.09	3.35	3.53	3.94	4.90
χ^2	0.840	0.820	0.802	0.872	0.734

TEM images at high magnification (Figures 3c and 3d) show the more detailed shape of the single STO and SLTO-0.025 particles. The images showed that the surface of cubic particles had sharp edges and flat surfaces. Figures 3e and 3f display the particle size distribution analysis, demonstrating that the particle sizes of the STO sample were in the range of 20–140 nm, with an average particle size of 72 nm.

On the other hand, the SLTO-0.025 sample had a particle size in the range of 20–80 nm, with an average particle size of 45 nm. This indicates that the La-doped $SrTiO_3$ has a smaller particle size than the undoped $SrTiO_3$ sample. The reduction in particle size of the SLTO-0.025 sample is attributed to the inhibitory effect of lanthanum on $SrTiO_3$ crystal growth. The inset images of Figures 3 (a) and (b) are SAED patterns that displayed bright spots for both samples, showing that the STO and SLTO-0.025 samples were polynanocrystalline.

The formation of $SrTiO_3$ nanocubes in a ethanol-isopropanol-water solution during synthesis consists of two main stages: nucleation and growth. Nucleation in aqueous reaction systems is driven by the amount of strontium cation (Sr^{2+}) and titanium hydroxyl anion ($[Ti(OH)_6]^{2-}$) in the alkaline solution. The amount of the $[Ti(OH)_6]^{2-}$ anion complex is maintained in the solution by stabilizing the hydroxyl groups of the Ti octahedra through an excess of OH^- ions. The excess OH^- ions are provided by adding NaOH and hydrolyzing the TBA in the solution. The alkaline environment facilitates the formation of a network of negatively charged titanium hydroxyl chains, thereby trapping the positively charged strontium cations through electrostatic attraction. This mechanism creates a reaction to form $SrTiO_3$ nuclei in solution [25]. The reaction mechanism is as follows:

$$Ti[OCH(CH_3)_2]_4 + 2C_2H_5OH + 3C_3H_7OH + 2NaOH \rightarrow [Ti(OH)_6]^{2-} + 2Na^+ + 5C_5H_{11}OH \quad (1)$$

$$[Ti(OH)_6]^{2-} + 2Na^+ + (1-x)Sr(NO_3)_2 + xLa(NO_3)_3 \rightarrow Sr_{1-x}La_xTiO_3 + 2Na^+ + xNO_3^- + 3H_2O \quad (2)$$

The growth stage was selectively controlled using CTAB as the capping surfactant. The positive charge of the (trimethylamine) head group allows adsorption through its coordination with oxygen anions during the crystal growth process. At the same time, the positive ions of the hydrolyzed TBA attach to the surface of the negatively-charged crystal faces through electrostatic interaction so that CTAB and TBA entirely cover the surface of the $SrTiO_3$ particles during the crystal growth and ripening process simultaneously [26]. The flawless confinement of the $SrTiO_3$ particles results in the oriented crystal growth and creates precipitates with a high ratio of the cubic-shaped particles. It was observed that the substitution of lanthanum affects the particle size of $SrTiO_3$, where the particle size became smaller in La-doped $SrTiO_3$ compared to undoped $SrTiO_3$ samples. The decrease in the particle size is associated with a reduction in the cell volume in the crystal structure, reducing the crystallite size of La-doped $SrTiO_3$. Nanocube particles with regular edges, flat surfaces, and sharp vertices generate intense interaction between the cubic particles through the large grain contact area, resulting in fewer pores in the compacted body of the samples.

The FT-IR spectrum of all samples (Figure 4) displayed the interaction of functional groups in the nanocube formation using CTAB and TBA by the appearance of absorption peaks at specific wavenumbers.

The presence of CTAB can explain these interactions, as the surfactant has a positive charge on the headgroups along with TBA, which contain positively charged amine groups directed towards the $SrTiO_3$ negatively charged crystal planes.

The presence of two peaks with weak intensities in the wavenumber range of 2920–2855 cm^{-1} indicates the asymmetric and symmetric C-H stretching vibrations in the methylene chains of the CTAB and TBA molecules [27].

 DOI: 10.15826/chimtech.2023.10.4.07

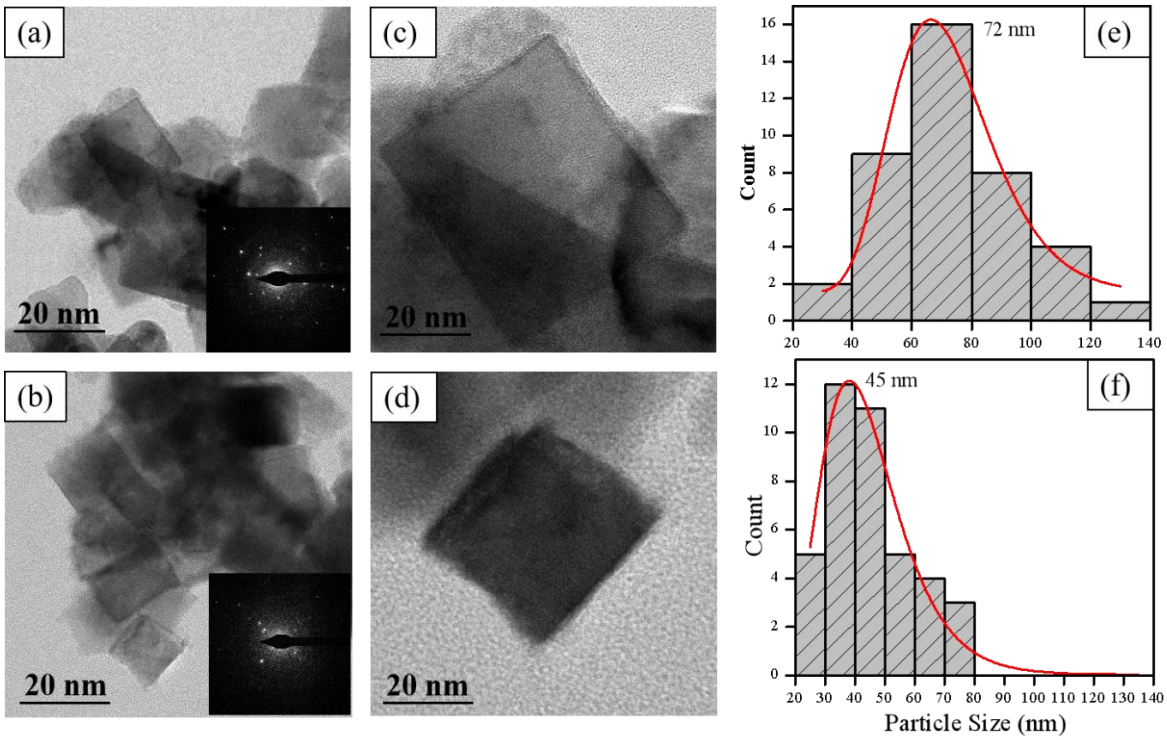

Figure 3 TEM images of $SrTiO_3$ particles STO (a) and SLTO-0.025 (b), larger magnification using HM-TEM (c, d), and particle size distribution of STO and SLTO-0.025 (e, f).

The surface interaction of $SrTiO_3$ particles with CTAB allows the scissoring vibrations of the CH_3-N^+ headgroup of the capping agent to cap the $SrTiO_3$ particles. These vibrations appear at the wavenumber 1463 cm^{-1}. The CTAB and TBA function was associated with controlling the shape and size of nanoparticles by capping the surface of $SrTiO_3$ particles. Nanoparticles have a large surface area with high surface energy leading to faster crystal growth and larger particle size. The presence of CTAB as a capping agent and TBA as a mineralizer reduces surface energy; thus, the particle growth process becomes slower and more directed [28].

Furthermore, the 500–850 cm^{-1} wavenumber range corresponds to the asymmetric stretching vibrations mode of Ti–O in the TiO_6 octahedra of perovskite structure [29]. The stretching that occurs towards a higher wavenumber as displayed in Figure 4 is caused by a decrease in the Ti–O vibrational frequency on the TiO_6 octahedra. This is related to the reduced unit cell volume, which results in shorter Ti–O bond lengths, weakening the vibrational frequency.

UV-vis diffuse reflection spectrum (UV-DRS) was measured to observe changes in the band gap energy (E_g) of $SrTiO_3$ samples due to lanthanum substitution. The UV-DRS of the $SrTiO_3$ samples is displayed in Figure 5.

The $SrTiO_3$ samples have a steep absorption edge in the UV absorption region with different absorption wavelengths. Significant absorption at shorter wavelengths is related to the smaller particle size distribution in the La-doped $SrTiO_3$ samples [30].

The E_g value was determined using UV-vis DRS data according to the Tauc-plot function from the plot of $(F(R^{\infty})\ h\upsilon)^n$ versus $h\upsilon$ with n = ½ by considering the indirect optical transition for $SrTiO_3$ samples.

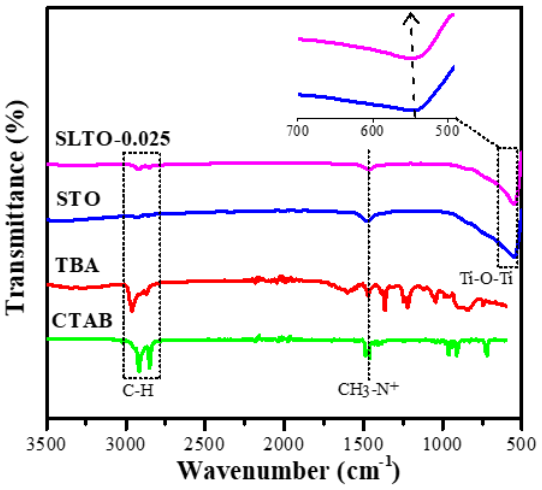

Figure 4 FTIR spectra of the STO and SLTO-0.025 samples.

The E_g value was estimated by a classical extrapolation approach according to: $(\alpha\ h\ v) = \beta\ (h\upsilon - E_g)^{½}$, where α is the absorption coefficient (cm^{-1}), h is the Planck's constant (J.s), υ is the frequency of the photon energy, β is a constant, and E_g is the band gap energy (eV), respectively [31]. The band gap energy of STO samples was estimated to be 3.17 eV and decreased after $SrTiO_3$ substitution by lanthanum to 3.13 eV. The decrease in the band gap energy value in the SLTO-0.025 sample is associated with adding electrons from lanthanum as an electron donor dopant.

The substitution of $SrTiO_3$ with electron-rich dopants generates the number of carriers and introduces delocalized electrons in the conduction band [32]. The large number of electron carriers creates a new energy level in the band gap. As a result, the energy band gap becomes narrower [33].

 DOI: 10.15826/chimtech.2023.10.4.07

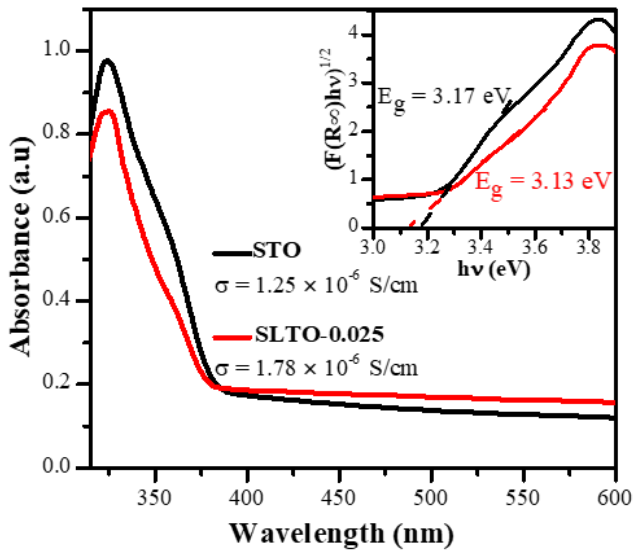

Figure 5 UV-vis reflectance spectra (DRS) and band gap energies of STO and SLTO-0.025 samples.

The electrical conductivity of $SrTiO_3$ samples was determined using LCR measurement with the frequency of 100 Hz at room temperature, and the value is displayed in Figure 5. The electrical conductivity of the STO sample is $1.25 \cdot 10^{-6}$ S/cm, and this value increases to $1.78 \cdot 10^{-6}$ S/cm after doping with 0.025 mole of lanthanum. The increase in electrical conductivity is related to the increase in the electron concentration, based on the following equation:

$$\sigma = en\mu, \quad (3)$$

where e is the electron charge (C), n is the electron concentration ($1/m^3$), and μ is the electron mobility ($m^2/V \cdot s$). This equation explains that the electrical conductivity is directly proportional to the number of electrons as carriers and electron mobility. In addition, an increase in the number of electrons in $SrTiO_3$ ceramics results in a narrowing of the band gap energy, making it easier for electrons to move from the valence band to the conduction band [34]. These excited electrons move freely along the conduction band to increase electrical conductivity. Introducing dopants into the $SrTiO_3$ lattice has shown its effect on modifying the electronic structure of $SrTiO_3$ and consequently improving the electrical properties. Higher valence doping can be used as a practical approach to improve the electrical performance of a material without significantly changing its physical properties.

4. Limitations

In this study, it was observed that $SrTiO_3$ doped with lanthanum was only effective at low concentrations, and $SrCO_3$ impurities were still present in the samples, resulting in low sample crystallinity. Therefore, future research will prioritize the refinement of synthesis parameters, including investigating variations in temperature, synthesis duration, and the concentration of starting materials, with the aim of producing samples with high crystallinity and the optimum lanthanum concentration.

5. Conclusions

La-doped $SrTiO_3$ nanocubes were successfully synthesized by the solvothermal method in a mixed solvent system of ethanol and isopropanol. XRD patterns and Le Bail refinement analysis of all samples indicate the successful substitution of lanthanum for strontium. The FT-IR spectrum revealed the interaction between CTAB and TBA molecules on the La-doped $SrTiO_3$ nanocube surfaces. TEM images show the effect of lanthanum on reducing the average particle size in SLTO-0.025 samples to 20–80 nm. The morphology of STO and SLTO-0.025 particles displayed flat surfaces and sharp edges. Furthermore, the band gap (E_g) in the SLTO-0.025 sample decreased slightly from the STO sample because of the presence of electrons derived from lanthanum as a dopant donor to the Sr^{2+}-sites in the SLTO-0.025 sample. The concentration of charge carriers (electrons) increased, so the reduced band gap energy (E_g) directly affects the electrical conductivity. The higher electrical conductivity, caused by the lower band gap energy value, is found in the SLTO-0.025 sample, caused by the lower band gap energy value. The effect of lanthanum doping on the crystal structure and morphology of $SrTiO_3$ nanocubes is associated with increased electrical conductivity, making it a potential thermoelectric material.

• Supplementary materials

No supplementary materials are available.

• Funding

This work was supported by the Directorate General of Higher Education, Research, and Technologyof the Ministry of Education, Culture, Research, and Technology of the Republic of Indonesia (grant no. 115/E5/PG.02.00.PL/2023).

• Acknowledgments

None.

• Author contributions

Conceptualization: Y.E.P.
Formal Analysis: Y.E.P., H.F., D.S., D.V.W.
Funding acquisition: Y.E.P.
Investigation: H.F.
Methodology: Y.E.P.
Project administration: H.F.
Supervision: Y.E.P., D.V.W.
Validation: Y.E.P., D.V.W., D.S.
Visualization: H.F.
Writing – original draft: Y.E.P.
Writing – review & editing: D.V.W., D.S.

• Conflict of interest

The authors declare no conflict of interest.

 DOI: 10.15826/chimtech.2023.10.4.07

• Additional information

Authors IDs:

Yulia Eka Putri, Scopus ID 55261197300;

Dedi Satria, Scopus ID 57200695552;

Diana Vanda Wellia, Scopus ID 35363286300.

Websites:

Andalas University, https://www.unand.ac.id/;

Muhammadiyah University of Sumatera Barat, https://www.umsb.ac.id/.

References

1. Putri YE, Said SM, Diantoro M. Nanoarchitectured titanium complexes for thermal mitigation in thermoelectric materials. Renewable Sustain Energy Reviews. 2019;101:346–360. doi:10.1016/j.rser.2018.10.006
2. Li J, Wu Q, Wu J. Synthesis of Nanoparticles via Solvothermal and Hydrothermal Methods. Handbook of Nanoparticles. Oak Ridge: Springer International Publishing; 2015. 1–28 p.
3. Liu J, Nie Y, Xue W, Wu L, Jin H, Jin G, et al. Size effects on structural and optical properties of tin oxide quantum dots with enhanced quantum confinement. J Mater Res Technol. 2020;9(4):8020–8028. doi:10.1016/j.jmrt.2020.05.041
4. Dresselhaus MS, Chen G, Tang MY, Yang R, Lee H, Wang D, et al. New directions for low-dimensional thermoelectric materials. Adv Mater. 2007;19:1043–1053. doi:10.1002/adma.200600527
5. Assirey EAR. Perovskite synthesis, properties and their related biochemical and industrial application. Saudi Pharmaceut J. 2019;27:817–829. doi:10.1016/j.jsps.2019.05.003
6. Amalraj AJJ, Wang S-F. Synthesis of transition metal titanium oxide ($MTiO_x$, M = Mn, Fe, Cu) and its application in furazolidone electrochemical sensor. J Ind Engin Chem. 2022;111:356–368. doi:10.1016/j.jiec.2022.04.018
7. Zhang B, Ru Q, Liu L, Wang J, Zhang Y, Zhao K, et al. Overcoming energy mismatch of metal oxide semiconductor catalysts for CO_2 reduction with triboelectric plasma. J Catal. 2023;419:1–8. doi:10.1016/j.jcat.2023.01.031
8. Xu S, Wang Q, Fan Z, Wang H, Liu G, Cui S. Analysis of fluorescence properties of novel Eu^{3+}-doped $ZnAl_2O_4$-based ceramic aerogels for high-power optical device applications. J Eur Ceram Soc. 2023;43:6337–6348. doi:10.1016/j.jeurceramsoc.2023.06.004
9. Fayaz U, Manzoor S, Dar AH, Dash KK, Bashir I, Pandey VK, et al. Advances of nanofluid in food processing: Preparation, thermophysical properties, and applications. Food Res Int. 2023;170:112954. doi:10.1016/j.foodres.2023.112954
10. Selvaraj P, Roy A, Ullah H, Devi PS, Tahir AA, Mallick TK, et al. Soft-template synthesis of high surface area mesoporous titanium dioxide for dye-sensitized solar cells. Int J Energy Res. 2018;1–12. doi:10.1002/er.4288
11. Zavjalov A, Tikhonov S, Kosyanov D. TiO_2-$SrTiO_3$ biphase nanoceramics as advanced thermoelectric materials. Mater. 2019;12:2895. doi:10.3390/ma12182895
12. Ibrahim IR, Matori KA, Ismail I, Rusly SNA, Nazlan R, Yusof NH, et al. Influence of nanometric microstructural development on thermophysical properties of lanthanum-doped strontium titanate. Mater Chem Phys. 2021;270:124867. doi:10.1016/j.matchemphys.2021.124867
13. Yeandel SR, Molinari M, Parker S. Nanostructuring perovskite oxides: The impact of $SrTiO_3$ nanocube 3D self-assembly on thermal conductivity. RSC Adv. 2016;6:114069–11477. doi:10.1039/C6RA23887D
14. Azevedo SA, Laranjeira JAS, Ururi JLP, Longo E, Sambrano JR. An accurate computational model to study the Ag-doping effect on $SrTiO_3$. Comput Mat Sci. 2022;214:111693. doi:10.1016/j.commatsci.2022.111693
15. Benthem K Van, Elsässer C, French RH. Bulk electronic structure of $SrTiO_3$: Experiment and theory. J Appl Phys. 2001;90(12):6156–6164. doi:10.1063/1.1415766
16. Nunocha P, Bongkarn T, Harnwunggmoung D, Tanusilp S, Suriwong T. Thermoelectric properties of La-doped A-site $SrTiO_3$ ceramics synthesised by the sol-gel auto-combustion technique. Mater Res Innovat. 2023;1–10. doi:10.1080/14328917.2023.2196479
17. Nunocha P, Kaewpanha M, Bongkarn T, Eiad-Ua A, Suriwong T. Effect of Nb doping on the structural, optical, and photocatalytic properties of $SrTiO_3$ nanopowder synthesized by sol-gel auto combustion technique. J Asian Ceram Soc. 2022;10(3):583–596. doi:10.1080/21870764.2022.2094556
18. Maity S, Kulsi C, Banerjee S, Das S, Chatterjee K. Dependence of thermoelectric power and electrical conductivity on structural order of PEDOT-Tos-graphene nanocomposite via charge carrier mobility. Mater Res Express. 2019;6:105095. doi:10.1088/2053-1591/ab3e7c
19. Zhang Y, Zhong L, Duan D. A single-step direct hydrothermal synthesis of $SrTiO_3$ nanoparticles from crystalline P25 TiO_2 powders. J Mater Sci. 2016;51:1142–1152. doi:10.1007/s10853-015-9445-7
20. Putri YE, Wendari TP, Rahmah AA, Refinel R, Said SM, Sofyan N, et al. Tuning the morphology of $SrTiO_3$ nanocubes and their enhanced electrical conductivity. Ceram Int. 2022;48:5321–5326. doi:10.1016/j.ceramint.2021.11.075
21. Dang F, Wan C, Park NH, Tsuruta K, Seo WS, Koumoto K. Thermoelectric Performance of $SrTiO_3$ Enhanced by Nanostructuring - Self-Assembled Particulate Film of Nanocubes. ACS Appl Mater Interfaces. 2013;5:10933–10937. doi:10.1021/am403112n
22. Park NH, Dang F, Wan C, Seo WS, Koumoto K. Self-originating two-step synthesis of core-shell structured La-doped $SrTiO_3$ nanocubes. J Asian Ceram Soc. 2013;1:35–40. doi:10.1016/j.jascer.2013.02.004
23. Knauss KG, Dibley MJ, Bourcier WL, Shaw HF. Ti(IV) hydrolysis constants derived from rutile solubility measurements made from 100 to 300°C. Appl Geochem. 2001;16:1115–1128. doi:10.1016/S0883-2927(00)00081-0
24. Rizwan M, Usman Z, Shakil M, Gillani SSA, Azeem S, Jin HB, et al. Electronic and optical behaviour of lanthanum doped $CaTiO_3$ perovskite. Mater Res Express. 2020;7:15920. doi:10.1088/2053-1591/ab6802
25. Chen KY, Chen YW. Preparation of barium titanate ultrafine particles from rutile titania by a hydrothermal conversion. Powder Technol. 2004;141:69–74. doi:10.1016/j.powtec.2004.03.002
26. Ma Q, Mimura K-I, Kato K. Diversity in size of barium titanate nanocubes synthesized by a hydrothermal method using an aqueous Ti compound. CrystEngComm. 2014;16:8398–8405. doi:10.1039/c4ce01195c
27. Putri YE, Andriani N, Wendari TP, Said SM, Wellia DV, Refinel, et al. Tunable morphology of strontium titanate nanocubes controlled by tert-butylamine-assisted solvothermal method and their enhanced electrical conductivity. Ceram Int. 2022;49(6):9909–9915. doi:10.1016/j.ceramint.2022.11.166
28. Jha K, Bhattarai A, Chatterjee SK. Surface Tension Studies on the Micellization of Cetyltrimethylammonium Bromide in Presence and Absence of KCl and NaCl in Aqueous Media at Room Temperature. Bibechana. 2014;10:52–57. doi:10.3126/bibechana.v10i0.9311
29. Yang D, Zou X, Sun Y, Tong Z, Jiang Z. Fabrication of three-dimensional porous La-doped $SrTiO_3$ microspheres with enhanced visible light catalytic activity for Cr(VI) reduction. Front Chem Sci Eng. 2018;12:440–449. doi:10.1007/s11705-018-1700-4
30. Doak J, Gupta RK, Manivannan K, Ghosh K, Kahol PK. Effect of particle size distributions on absorbance spectra of gold nanoparticles. Physica E. 2010;42(5):1605–1609. doi:10.1016/j.physe.2010.01.004
31. Nunocha P, Kaewpanha M, Bongkarn T, Phuruangrat A. A new route to synthesizing La-doped $SrTiO_3$ nanoparticles using the

 DOI: 10.15826/chimtech.2023.10.4.07

sol-gel auto combustion method and their characterization and photocatalytic application. Mater Sci Semiconductor Process. 2021;134:106001. doi:10.1016/j.mssp.2021.106001
32. Tong Y, Gao P, Xu J, Liu S, Yang Y, Wang Y, et al. Cobalt doped nitrogen-vacancies-rich C_3N_5 with optimizing local electron distribution boosts peroxymonsulfate activation for tetracycline degradation: Multiple electron transfer mechanisms. Chemosphere. 2023;339:139549. doi:10.1016/j.chemosphere.2023.139549
33. Anjum S, Ilayas T, Mustafa Z. Influence of antimony substitution on structural, magnetic and optical properties of cadmium spinel ferrite. Appl Phys A. 2020;126:227. doi:10.1007/s00339-020-3407-x
34. Łącz A, Drożdż E. Porous Y and Cr–doped $SrTiO_3$ materials—electrical and redox properties. J Solid State Electrochem. 2019;23:2989–2997. doi:10.1016/j.physe.2010.01.004

 DOI: 10.15826/chimtech.2023.10.4.07